



# NO Adsorption and Removal at Low Temperature by Adsorption Catalyst (Ce–Fe–Mn/ACFN)

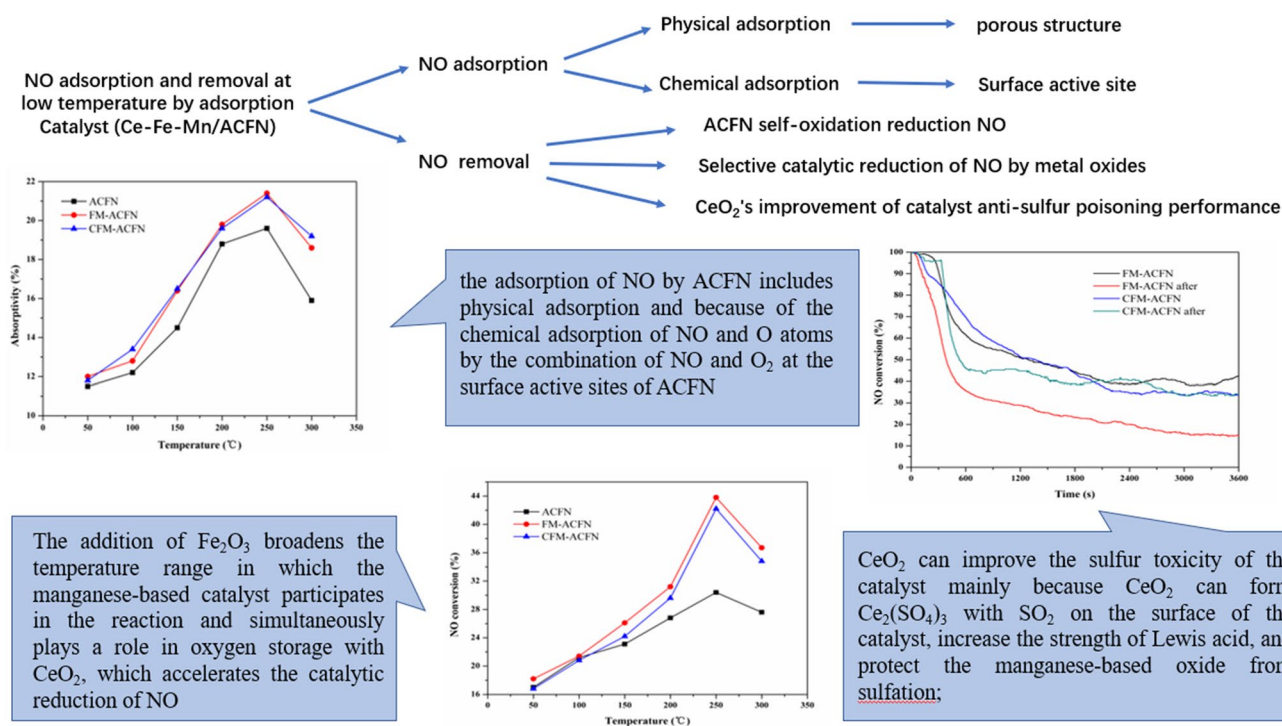
Boru Zhang<sup>1</sup> · Weijun Liu<sup>1</sup> · Furong Liang<sup>1</sup> · Shuhua Zhang<sup>2</sup>

Received: 4 March 2019 / Accepted: 7 June 2019 / Published online: 24 June 2019  
© Springer Science+Business Media, LLC, part of Springer Nature 2019

## Abstract

FM/ACFN and Ce-doped CFM/ACFN low-temperature catalysts are prepared by an impregnation method that takes polyacrylonitrile-based activated carbon fiber modified with nitric acid as the carrier. The catalysts are characterized by X-ray diffraction, scanning electron microscopy, Fourier-transform infrared spectroscopy, and thermogravimetric analysis. The effects of temperature, oxygen, and sulfur dioxide on the adsorption and removal of NO by catalyst are studied by laboratory gas distribution. Results show that the addition of metal oxide can increase the ability of chemical adsorption of NO by ACFN by 2.5%, and the ability of catalytic reduction of NO can be increased by up to 14%. Under the condition of oxygen and ammonia as reducing agent at 250 °C, the ability of metal-oxide-loaded ACFN to catalyze the reduction of NO can reach up to 68%. The addition of Ce does not completely inhibit the decrease of the ability of the catalyst in treating NO under sulfur-containing conditions, but it can maintain the catalyst's reducing ability at a relatively stable level, and the presence of SO<sub>2</sub> will reduce the redox capacity of ACFN itself.

## Graphic Abstract



Extended author information available on the last page of the article

**Keywords** Adsorption catalyst · Low-temperature denitrification · Sulfur poisoning · Activated carbon fiber (ACF) · NO storage and reduction technology (NSR)

## 1 Introduction

$\text{NO}_x$  storage and reduction technology (NSR) is a method of gas-exhausting treatment based on the selection of catalytic reduction technology (SCR) to better solve the  $\text{NO}_x$  emission of lean-burn engines. The NSR reaction mainly includes the following steps: NO is oxidized to  $\text{NO}_2$ ,  $\text{NO}_2$  is stored in the active site of the catalyst in the form of  $\text{NO}_3^-$ ,  $\text{NO}_x$  is desorbed from the catalyst when the reducing agent is introduced, and then is reduced to  $\text{N}_2$  by the reducing agent [1]. The NSR catalyst mainly comprises a carrier and a catalyst.

Activated carbon fiber (ACF), as a high-efficiency adsorbent for environmental pollution prevention and gas purification, not only occupies a major position in the treatment of fixed exhaust emissions but recently has been explored by a number of scientists as to whether it can be applied to reduce mobile pollution sources such as automobiles and ships. Compared with alumina, ACF with a diameter of 10–30  $\mu\text{m}$  has greater advantages as a catalyst carrier due to it having a high specific surface area, not existing in ACF, which can load more metal oxides. Large pores, a small number of transition pores, and micropores are present on the surface of the fiber, and the adsorbed material does not need to pass through large pores, transition pores, or even small pores in sequence, which obviously demonstrates its good adsorption performance [2, 3].

Catalysts, such as  $\text{MnO}_2/\text{Al}_2\text{O}_3$ ,  $\text{MnO}_x/\text{NaY}$ , and  $\text{MnO}_x/\text{TiO}_2$ , with transition-metal manganese oxide as active components, have also received widespread attention due to their advantage of low-temperature SCR activity. Yoshikawa et al. [4] studied the effect of low-temperature treatment of  $\text{NO}_x$  when  $\text{Mn}_2\text{O}_3$  was loaded onto activated carbon fiber. It was found that when the loading of  $\text{Mn}_2\text{O}_3$  was 15%, the temperature increased in the temperature range 50–250 °C. The better the NO treatment effects, a conversion rate of 90% or more was achieved at 150 °C. Huang et al. [5] found that the addition of iron can increase the reaction rate of  $\text{Mn}_2\text{O}_3$ , and its reactivity at lower temperatures also increased. A large number of studies have found that the addition of  $\text{Fe}_2\text{O}_3$  can increase the specific surface area and pore volume of the catalyst. The particle surface distribution of the catalyst is made uniform, and the temperature catalytic range is enlarged to improve the catalyst activity. Wu et al. [6] prepared  $\text{MnO}_x/\text{TiO}_2$  catalyst modified by  $\text{CeO}_2$  in a sol–gel method for the study of selective catalytic reduction of low-temperature ammonia and investigated the effect on catalytic performance. At 150 °C, the space velocity is 40,000  $\text{h}^{-1}$ ; after adding 3%  $\text{O}_2$  and 100-ppm  $\text{SO}_2$ , the conversion of NO to  $\text{MnO}_x/\text{TiO}_2$  catalyst is reduced from 95% to 30% in

45 min. Under the same conditions, for  $\text{CeO}_2\text{-MnO}_x/\text{TiO}_2$ , the rate of conversion remained above 84%, indicating that the addition of  $\text{CeO}_2$  significantly improved the sulfur resistance of the catalyst.

In this paper, we intend to find a high-efficiency  $\text{NO}_x$  removal catalyst for low-temperature anti-sulfur poisoning. The polyacrylonitrile-based ACF modified with nitric acid is used as a carrier to prepare FM/ACF and Ce-doped CFM/ACF catalysts. The catalysts are characterized by X-ray diffraction (XRD), scanning electron microscopy (SEM), Fourier-transform infrared (FTIR) spectroscopy, X-ray photoelectron spectroscopy (XPS), Temperature Programmed Desorption (TPD), and thermogravimetric-differential thermal analysis (TGA). The effects of temperature, oxygen, and sulfur dioxide on adsorption and removal of NO by catalyst are studied by laboratory gas distribution.

## 2 Experimental Section

### 2.1 Materials

Polyacrylonitrile-based ACF felt was obtained from Shanghai Rumble Industrial Co., Ltd. (China).  $\text{HNO}_3$ ,  $\text{Mn}(\text{NO}_3)_2$ ,  $\text{Fe}_2(\text{NO}_3)_3$ , and  $\text{Ce}(\text{NO}_3)_3$  chemical reagents were procured from Shanghai Titanchem Co., Ltd. (China).

### 2.2 Pre-treatment of ACF

In the experiment, ACF was treated with nitric acid, cut into small wafers with diameters of 2.5 cm, and washed with deionized water three to four times. Then, deionized water was added every 30 min and boiled for 2 h. Next, the wafers were acidified with 60% nitric acid at room temperature for 2 h, washed to neutral, then dried in air; drying should be done in an oven at 100–120 °C to obtain nitric-acid-modified carbon fiber felt (ACFN).

### 2.3 Preparation of CFM-ACFN and FM-ACFN

The catalyst was prepared by the isovolumetric impregnation method: The  $\text{Mn}(\text{NO}_3)_2$  and  $\text{Fe}(\text{NO}_3)_3$  solutions with  $\text{Mn}^{2+}$  and  $\text{Fe}^{3+}$  molar ratios of 1:1 were removed, the deionized water was placed in a certain ratio to form an immersion liquid, and the volume was immersed to a certain amount of ACFN. The total mass of the metal oxide was 20% of the mass of the carrier. In the Ce-doped catalyst, the masses of Mn and Fe oxide were 15% of the mass of the carrier, and the oxide of Ce was 5% of the mass of the carrier. The

beaker containing the masses was sealed with plastic wrap and placed in a constant-temperature water-bath shaker. After stirring at a speed of 80 rpm for 1 h at room temperature, it was allowed to stand for 1 h at 65 °C and 110 °C for 6 h. Finally, the catalyst was prepared by calcination at 350 °C for 6 h in nitrogen atmosphere.

In the experiment, to compare the test results, three sets of catalysts were set up for testing and comparison. The first group was ACF modified only by nitric acid, designated ACFN, and the second group was modified ACF loaded with  $\text{MnO}_2$  and  $\text{Fe}_2\text{O}_3$ , designated FM-ACFN. The third group was modified ACF loaded with  $\text{CeO}_2$ ,  $\text{MnO}_2$ , and  $\text{Fe}_2\text{O}_3$ , and designated CFM-ACFN.

## 2.4 Characterization

In this experiment, the surface morphology of the catalyst was observed using a Hitachi SU8010 scanning electron microscope. The test parameters were as follows: amplification factor, 5–10 K times; acceleration voltage, 0.1–30 kV; and low-vacuum-pressure range, 1–270 Pa. The samples were characterized using a German D-2 HASER X-ray diffractometer. The test conditions were as follows: Cu target,  $K\alpha$  ray; tube voltage, 40 kV; tube current, 200 mA; scanning range, 10–80°; and step size  $2\theta$ , 0.02°.

Using an SII TG/DTA6300 thermogravimetric-differential thermal analyzer (Tokyo, Japan), the change of mass fraction of different catalysts in the temperature range 50–600 °C was studied under the condition of pure  $\text{N}_2$  at a heating rate of 5 °C/min. The thermogravimetric-differential analyzer was used in conjunction with a Nicolet iS10 FTIR spectrometer (TG-FTIR) (Waltham, USA) to qualitatively

**Table 1** Simulating gas intake under different operating conditions

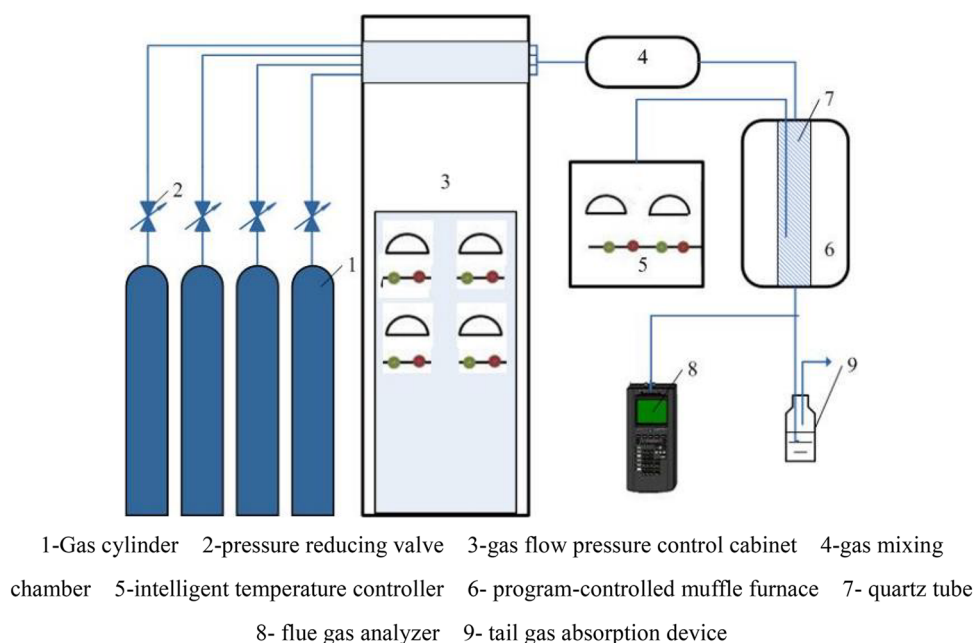
Condition	Air input ( $\text{Nml min}^{-1}$ )				
	$\text{N}_2$	NO	$\text{NH}_3$	$\text{O}_2$	$\text{SO}_2$
NO	997.5	2.51	–	–	–
$\text{NO} + \text{O}_2$	966.25	2.51	–	31.5	–
$\text{NO} + \text{NH}_3$	994.13	2.51	3.75	–	–
$\text{NO} + \text{O}_2 + \text{NH}_3$	962.88	2.51	3.75	31.5	–
$\text{NO} + \text{O}_2 + \text{NH}_3 + \text{SO}_2$	900.38	2.51	3.75	31.5	62.5

analyze the components of the catalyst released at different temperature stages. The pore-structure parameters of ACFs were determined using an ASAP 2020 (Micromeritics, USA) specific surface area and pore-size analyzer. The sample was subjected to denitrification treatment at 110 °C,  $1.3 \times 10^{-2}$  Pa, the test temperature was 77.4 K, and the relative pressure was  $10^{-6}$ –1 Pa. The oxygen- and nitrogen-containing functional groups on the surface of the ACFs were tested using an XSAM800 photoelectron spectrometer (Kratos, UK).

## 2.5 Denitrification Activity Test

To simulate the exhaust emissions composition of a diesel engine under low-temperature conditions and test the denitrification efficiency of the catalyst in a fixed reaction vessel, the test reaction device used is shown in Fig. 1. The inner diameter of the reactor is 2.5 cm, the experimental gas space velocity is  $10,000 \text{ h}^{-1}$ , and the total gas-flow rate is  $1000 \text{ ml min}^{-1}$ . The intake air amount of the simulated flue gas passing through the mass-flow meter under different working conditions is shown in Table 1.

**Fig. 1** Schematic diagram of experiment system device



The mass of catalyst can be calculated according to

$$m = \frac{60\rho V}{W_V}, \quad (1)$$

where  $W_V$  represents the volume space velocity ( $\text{h}^{-1}$ ),  $V$  the standard state of the gas-volume flow rate ( $\text{cm}^3 \text{min}^{-1}$ ),  $\rho = 0.085 \text{ g cm}^{-3}$  was the catalyst density, and  $m$  denotes catalyst quality (in g).

The removal rate of  $\text{NO}_x$  is taken as the evaluation index of the results in this experiment. The mixture concentration at the outlet was detected by an MGA5 comprehensive flow gas analyzer, and the removal rate of the related gas is expressed as follows:

$$\xi = \frac{C_{Ai} - C_{A0}}{C_{Ai}} \times 100, \quad (2)$$

where  $\xi$  represents the gas-removal efficiency (in %), and  $C_{Ai}$  and  $C_{A0}$  denote import- and export-gas concentration (in ppm), respectively. In the study of the adsorption of NO on the catalyst,  $\xi$  represents the gas-adsorption efficiency (in %).

## 3 Results and Discussions

### 3.1 XRD Characterization of Modified ACF

Figure 2 shows the XRD spectra of two samples, ACF and ACFN. The two sample spectra exhibit two distinct reflection peaks at  $\theta$  angles of approximately  $25^\circ$  and  $44^\circ$ .

The lateral size ( $L_a$ ) and stacking height ( $L_c$ ) of ACF and ACFN in Fig. 2 are calculated by the Scherrer equation as follows:

$$L_c = \frac{k_c \lambda}{\beta_{002} \cos \theta}, \quad (3)$$

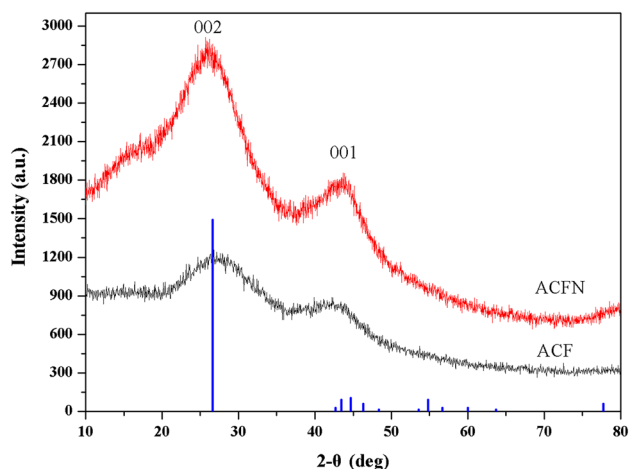


Fig. 2 XRD diagram of nitric acid modified ACF

$$L_a = \frac{k_a \lambda}{\beta_{001} \cos \theta}, \quad (4)$$

where the Scherrer constants,  $k_c$  and  $k_a$ , are 0.9 and 1.77, respectively [7];  $\lambda$  is the X-ray wavelength, 0.154 nm;  $\beta_{001}$  and  $\beta_{002}$  are the full widths at half-maxima (FWHM) (in deg), which should be converted into radians in the calculation; and  $\theta$  is the diffraction angle (in deg). The results are summarized in Table 2.

Although ACF is one of the amorphous carbon materials, it has a layered structure formed by a hexagonal annular plane of carbon atoms in its structure; the arrangement is disordered and irregular, the crystal formation is defective, and the crystal grains are minute and contain a small amount of impurities. It should be noted that a large change occurs in  $L_a$  and  $L_c$  after the modification, indicating that there is a significant increase in the size of the crystallites in the ACF, but it does not exclude the changes in peak shape caused by the effects of lattice distortion and internal stress. Another reason for the two peaks becoming stronger is that the nitric acid treatment removes some of the impurities in the ACF, which improves its purity.

### 3.2 XPS Characterization of Modified ACF

The XPS full scan of the ACF and ACFN samples is shown in Fig. 3.

The relative areas of the peaks indicate their relative contents on the ACF surface. By calculating the area, the relative contents of elemental C, N, and O on the ACF surface before and after modification are determined and are given in Table 3.

It can be seen from the table that the nitrogen content in the ACF after nitric acid modification is reduced by nearly one-third compared with that in the previous experiment due to washing several times after nitrification, and the surface oxygen content is increased from the previous ratio of 12.98% to 14.01%, in agreement with Ref. [8]. To further investigate the existence and relative content of ACF surface functional groups before and after modification, XPS single scans were performed on the N 1s and C 1s peaks of ACF and ACFN, as shown in Figs. 4 and 5, respectively. The binding energies of C–C, hydroxyl (C–O), carbonyl (C=O), and carboxyl (COOH) on the surface of ACF are 284.3, 285.0, and 286.5, 288.5 eV, respectively, and the binding energies of pyrimidine, pyrrole, and quaternary nitrogen in the nitrogen-containing functional group are 398.5, 400.5, and 401.2 eV, respectively [9]. Tables 4 and 5 list the relative contents of oxygen- and

Table 2  $L_a$ ,  $L_c$  values of ACF and ACFN

Sample	$L_c$ (nm)	$L_a$ (nm)
ACF	0.624	1.437
ACFN	1.94	2.04

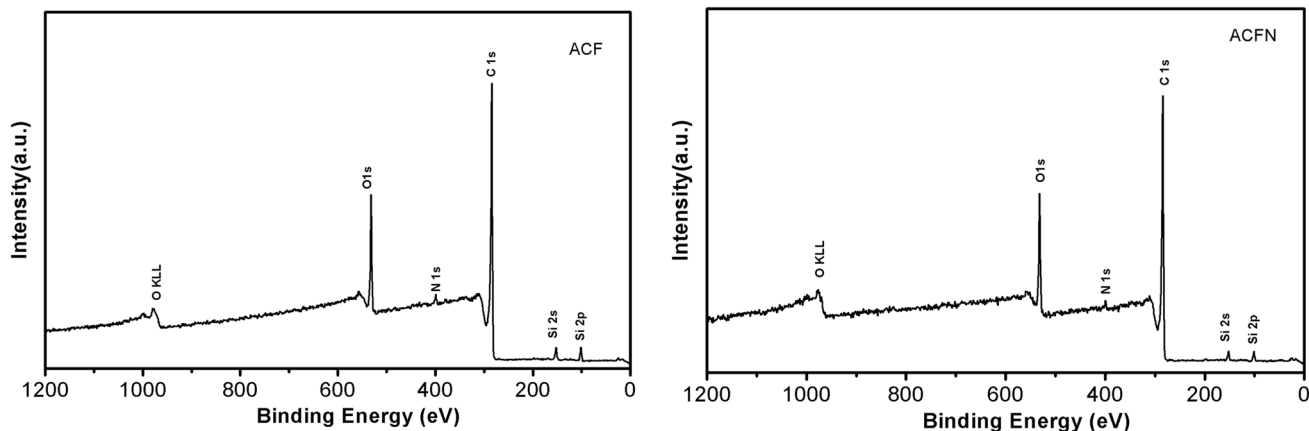


Fig. 3 XPS full scan spectrum of ACF and ACFN

**Table 3** Element contents in ACF and ACFN

Sample	C/%	N/%	O/%
ACF	85.42	1.60	12.98
ACFN	84.97	1.01	14.01

nitrogen-containing functional groups, respectively, on the surfaces of the two samples.

When the ACF is treated with nitric acid, the percentage of C–O functional group content on the surface is increased by 4.84%, and the percentage of C=O bonding is increased by 2.02%. The increase of these functional groups makes the surface of the ACF contain more oxidation sites. The adsorbed NO reacts with the oxygen-containing functional group on the surface of the ACF to form a functional group such as  $-\text{NO}_2$ , which vacates the adsorption site, resulting in an increase in the chemical adsorption efficiency of ACF for NO.

Results show that the presence of nitrogen-containing functional groups is powerful for enhancing the chemical adsorption of  $\text{SO}_2$  by ACF, especially theazole-functional compounds that play a major role in adsorbing  $\text{SO}_2$ . Because N on the pyrrole-like ring contains a lone pair of electrons, it has a strong basicity and a strong adsorption affinity for acid gases [10]. The specific adsorption process is as follows:  $\text{SO}_2$  reacts with  $\text{O}_2$  to form  $\text{SO}_3$ , and  $\text{SO}_3$  reacts with pyrrole to form a complex; the complex then promotes the sulfonation reaction of pyrrole and the formation of pyrrole sulfonic acid. The pyrrole sulfonic acid is easily hydrolyzed in an acidic environment to cause the sulfonic acid to fall off [11]. The content of pyrrole on the surface of ACFN modified by nitric acid decreased from 31.45% to 18.95%, a decrease of 12.5%. Therefore, the efficiency of chemical adsorption of  $\text{SO}_2$  by ACFN under both nitrogen- and sulfur-containing conditions is lower than that of ACF, which reduces the competitive

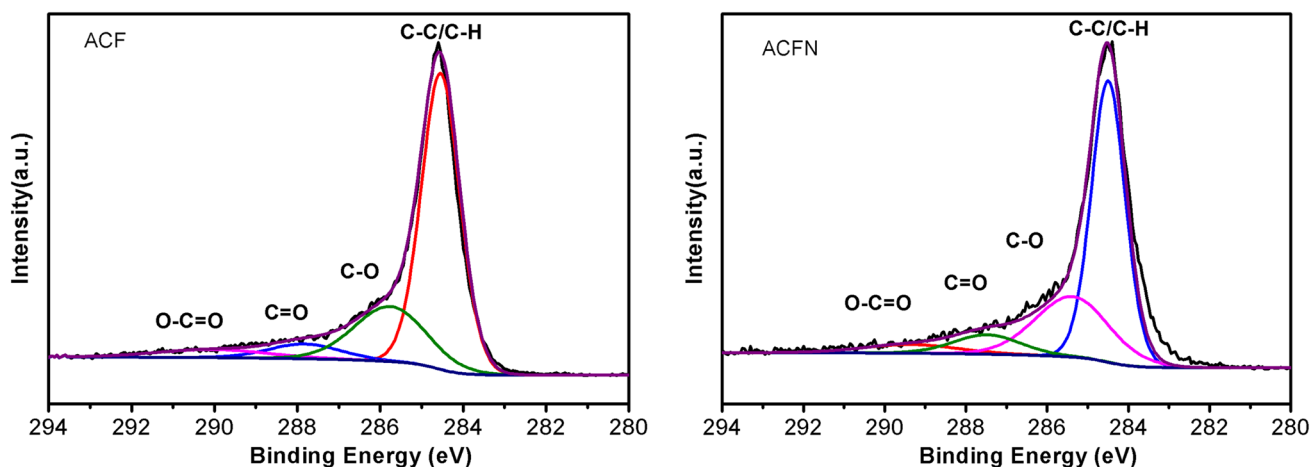


Fig. 4 C1s spectrum of ACF and ACFN

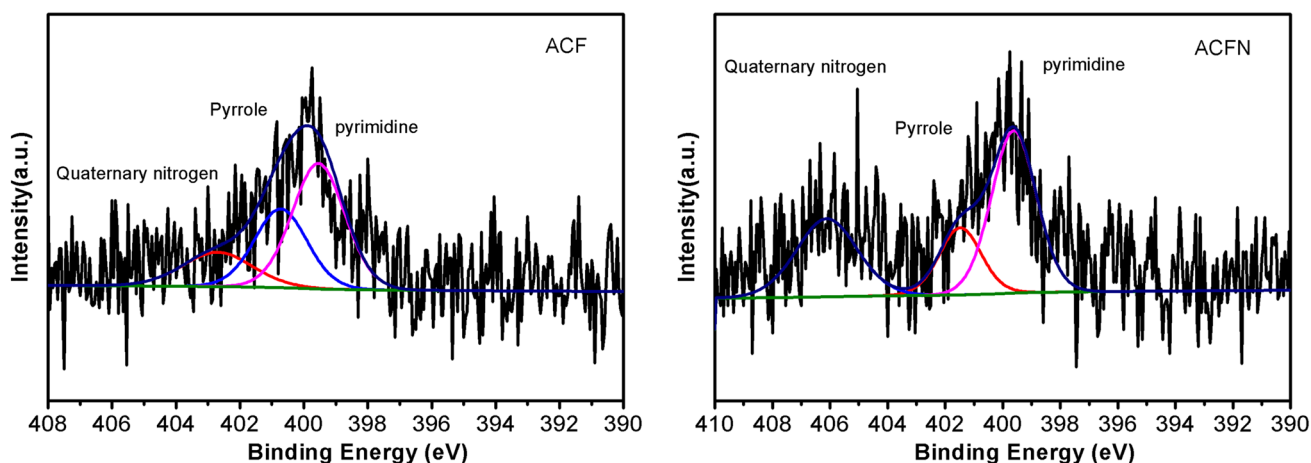


Fig. 5 N1s spectrum of ACF and ACFN

**Table 4** Percentage of oxygen-containing functional groups

Sample	Percentage of oxygen-containing functional groups/%			
	C–C/C–H	C–O	C=O	O–C=O
ACF	65.85	22.86	6.08	5.21
ACFN	59.10	27.70	8.10	5.10

**Table 5** Percentage of nitrogen-containing functional groups

Sample	Percentage of nitrogen-containing functional groups/%		
	Pyrimidine	Pyrrole	Quaternary nitrogen
ACF	50.19	31.45	18.36
ACFN	49.08	18.95	31.98

adsorption of  $\text{SO}_2$ , and is thus advantageous for the denitrification treatment of the catalyst.

### 3.3 Thermogravimetric Analysis of Three Different Catalysts

The prepared ACFN, FM-ACFN, and CFM-ACFN samples are separately placed in the analyzer for thermogravimetric analysis. The experimental conditions were heating to  $550\text{ }^\circ\text{C}$  at a heating rate of  $5\text{ }^\circ\text{C}/\text{min}$  under the action of  $100\text{ ml}/\text{min}$  nitrogen shielded gas; the results obtained are shown in Fig. 6.

Since ACF has strong water-absorbing ability in air, the moisture in ACFN at a temperature lower than  $100\text{ }^\circ\text{C}$  evaporates, so the catalyst quality rapidly decreases in

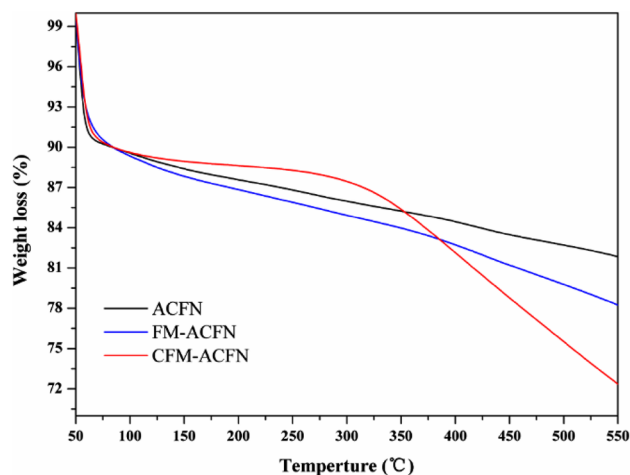


Fig. 6 variation of three different catalysts with temperature and mass

the range  $50\text{--}100\text{ }^\circ\text{C}$ . The XPS results reveal that there is an oxygen-containing group on the surface of ACF that increased after nitric acid treatment. Therefore, even in an oxygen-free environment, when the temperature is higher than  $100\text{ }^\circ\text{C}$ , ACFN itself began to oxidatively decompose. It can be seen from Fig. 6 that in the temperature range below  $300\text{ }^\circ\text{C}$ , the decomposition rate is small, and the mass change is less than 4%. When  $\text{MnO}_2$  and  $\text{Fe}_2\text{O}_3$  are added, the metal oxide acts as a catalyst to accelerate the oxidative decomposition reaction of ACFN itself. However, when  $\text{CeO}_2$  is added, ACFN is decomposed by itself in the low-temperature stage below  $300\text{ }^\circ\text{C}$ , and the mass change is less than 2%. When the temperature increases again, the rate of ACFN oxidative decomposition in CFM-ACFN is significantly improved. Therefore, CFM-ACFN is more suitable as a low-temperature adsorption catalyst.

### 3.4 SEM and BET Characterization of Different Catalysts

The catalysts at different test stages are characterized by SEM in the experiment, and the results are shown in Fig. 4.

It can be clearly seen from the SEM images of the catalysts in different experimental stages (Fig. 7) that the industrial grade ACF surface has many impurities, and the impurities attached to the fiber surface are basically removed by nitric acid modification, which validates the XPS result of N content decreasing from 1.60% to 1.01%. As can be seen from Fig. 7c, the metal oxide in the laboratory-prepared catalyst can be uniformly and finely attached to the surface of ACFN to form crystals. As can also be seen from Fig. 7d, when the catalyst sulfur is poisoned, these metal oxides become sulfates, which disappear in a significant volume from the surface of ACFN, which is the direct cause of the decrease in the catalytic ability of the catalyst.

At the same time, the pore structure on the surface of ACF and ACFN was observed by SEM, and the results are shown in Fig. 8. Although it was still difficult to observe the presence of pores at the maximum magnification of the scanning electron microscope, BET characterization of ACF and

ACFN was performed, and the results are shown in Table 6 and Fig. 9.

As shown in Fig. 9, ACF exhibits a significant pore-volume increase in the range of pore sizes  $< 0.5$  nm, indicating that the surface contains a large number of micropores, while the distribution of mesopores and macropores is smaller. The interlayer structure of surface graphite-like crystallites after ACF treatment with nitric acid tends to be regular, and the pores of the interlayer shrink, resulting in a lower pore-volume increase at a larger pore size.

The characterization of the above pore structure revealed that the pore structure and pore parameters of ACF did not change much after nitric acid treatment, and the interference of pore structure was excluded from the factors affecting the adsorption of NO by the catalyst.

### 3.5 TG-FTIR Characterization of Different Adsorbed NO Catalysts

The ACFN and CFM-ACFN catalysts for saturated adsorption of NO were separately analyzed by TG-FTIR under anaerobic conditions. The specific experimental conditions were as follows: 100 ml/min nitrogen shielding gas; heating

Fig. 7 SEM diagram of different catalysts

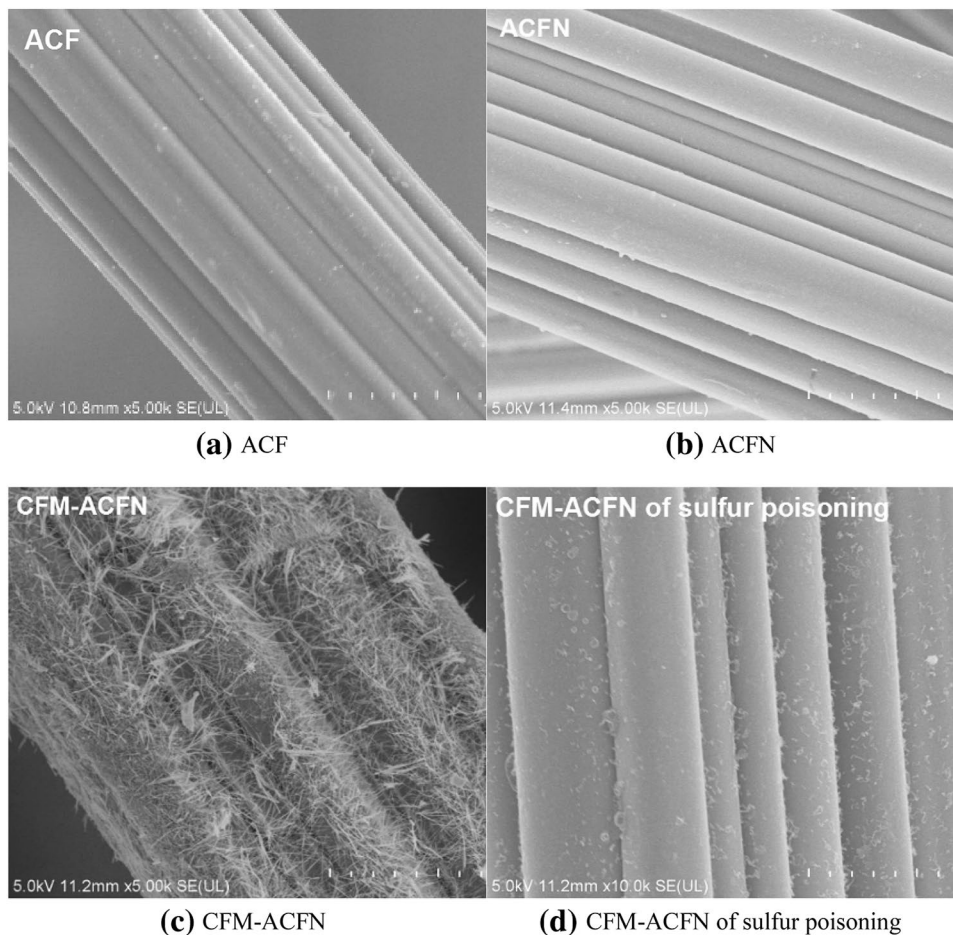


**Fig. 8** SEM spectrum of 200 k times magnification of different catalysts

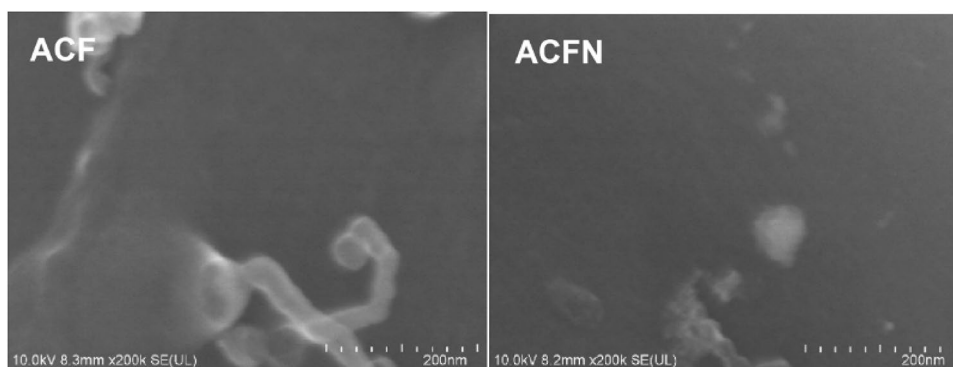


**Table 6** Physical properties of different catalysts

Catalyst	BET surface area (m <sup>2</sup> /g)	Pore volume (×10 <sup>-2</sup> m <sup>3</sup> g <sup>-1</sup> )	Thickness (nm)
ACF	1178.91	0.7487	2.15
ACFN	1275.12	0.7621	2.03

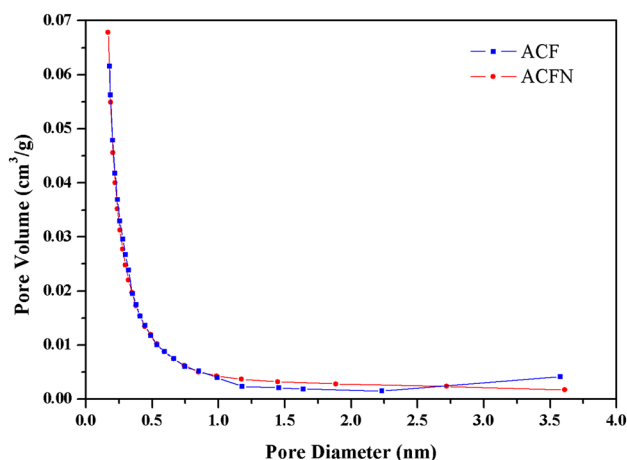
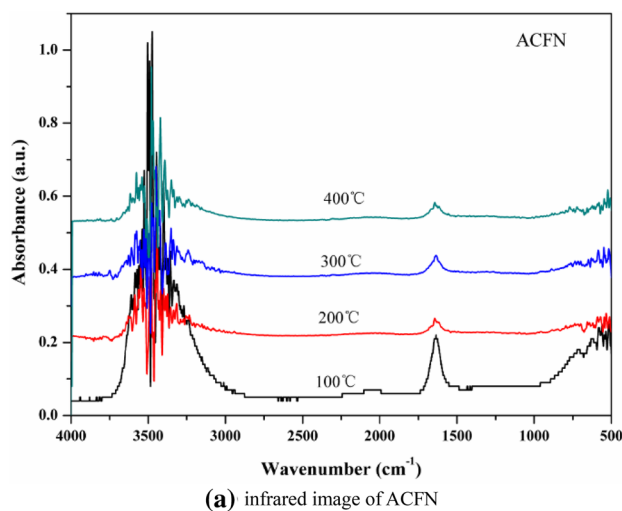


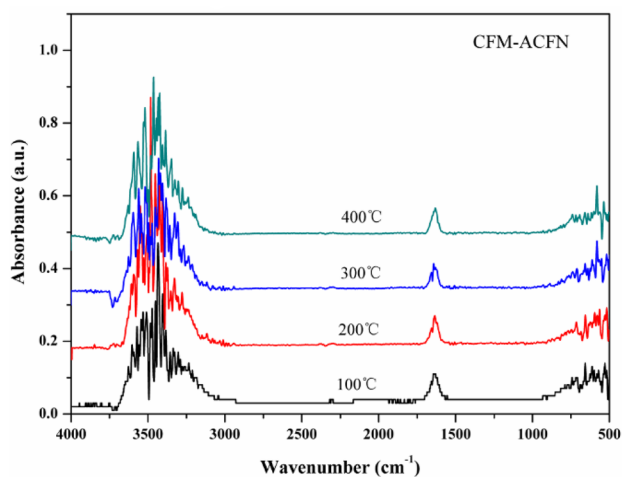
**Fig. 9** Pore size distribution of different catalyst surfaces

rate is increased to 500 °C at 5 °C/min; and infrared data extracted at 100 °C, 200 °C, 300 °C, and 400 °C. The results are shown in Fig. 10.

According to Fig. 10, referring to the infrared spectrum comparison table, it can be concluded that increasing the amount of metal oxide does not change the kind of gas released by ACFN after the heating reaction. In the 100 °C stage, there is a small convex peak at 2000–2250 cm<sup>-1</sup>, indicating that there is CO gas released at this time. There is a small peak in the 3500–3980 cm<sup>-1</sup> phase, indicating that the gas after the reaction also contains a certain amount of H<sub>2</sub>O. When the temperature exceeds 100 °C, the CO corresponding peak disappears. In the entire stage of 100–400 °C, the peaks of the following ranges are included: 1550–1750 cm<sup>-1</sup>



**(a)** infrared image of ACFN



**(b)** infrared image of CFM-ACFN

**Fig. 10** Infrared absorption spectra of substances released by catalysts at different temperatures

(NO<sub>2</sub>), 3580–3800 cm<sup>-1</sup> (NO), 640–700 cm<sup>-1</sup> (CO<sub>2</sub>), and 3550–3750 cm<sup>-1</sup> (CO<sub>2</sub>), indicating that ACF can partially oxidize NO to NO<sub>2</sub> and self-oxidize to form CO and CO<sub>2</sub> in ACFN self-adsorption and reduction of NO. At the same



time, the following reactions of ACF to remove NO may also exist in the reaction:



Since the experiment is carried out in a pure  $\text{N}_2$  environment, it is impossible to analyze the cause of formation of  $\text{N}_2$ , and it is not possible to accurately judge whether or not reactions (5) and (6) exist according to Fig. 10, and the above reactions are to be further studied.

At the same time, considering that ACF and ACFN will contain a large amount of water at low temperature, NO and  $\text{NO}_2$  are easily combined with water to form  $\text{HNO}_2$  and  $\text{HNO}_3$ , which will have a certain influence on the performance test of adsorbing NO. Therefore, in all adsorption and selective catalytic reduction tests, all catalyst samples must be dehydrated in a muffle furnace for 2 h, at 80 °C, and the test samples stored in a dry box.

### 3.6 NO Adsorption and Desorption by Different Catalysts

The NO concentration in the exhaust emissions was observed separately when the catalyst reached stable adsorption within 1 h, in the pure  $\text{N}_2$  environment, and only NO gas was introduced. The NO adsorption efficiency of the catalyst is calculated by formula (2), and the results are shown in Fig. 11.

According to Fig. 11, ACFN itself has a certain adsorption capacity for NO, and the adsorption efficiency is the highest at 250 °C, which can reach 19.5%, but the adsorption efficiency decreases with increasing temperature. This is because the adsorption of NO by ACFN includes physical adsorption and because of the chemical adsorption of NO and O atoms by the combination of NO and  $\text{O}_2$  at the surface active sites of ACFN [12]. When the temperature is too high, the physically adsorbed NO is released, so the adsorption capacity of ACFN for NO decreases at 300 °C. The loading of metal oxide increased the surface active site of ACFN, which led to an increase in the chemical adsorption capacity of CFM-ACFN and FM-ACFN for NO. At this time, the adsorption efficiency of CFM-ACFN and FM-ACFN for NO reached 21.5% at 250 °C. However, the addition of metal oxide does not affect the physical adsorption performance of ACFN for NO. Therefore, as the temperature increases again, the NO in the physically adsorbed state is released, and the adsorption efficiency of CFM-ACFN and FM-ACFN for NO also decreases.

In the experiment, NO and  $\text{NH}_3$  gases were injected into the pure  $\text{N}_2$  environment at the same time. The concentration of NO in the discharged gas is observed when the catalytic treatment effect of NO is stable within 1 h. The efficiency of

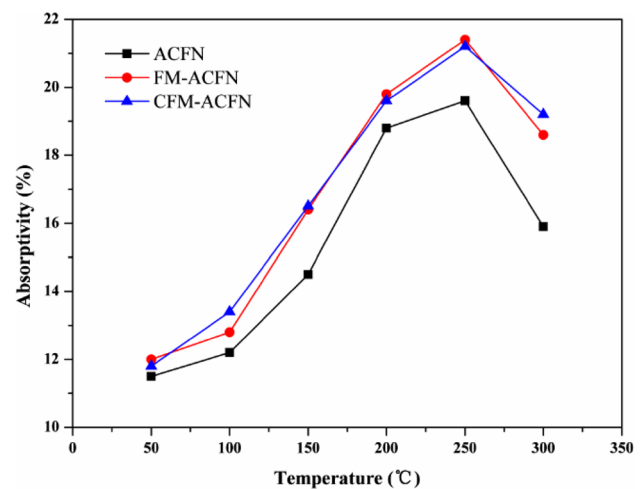


Fig. 11 Comparison of adsorption efficiency of NO on different catalysts

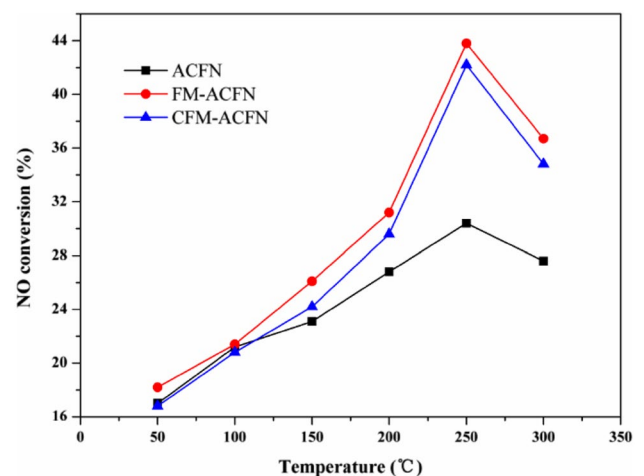
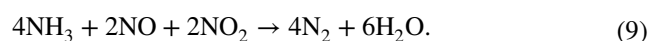
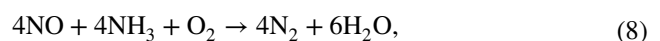
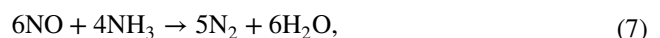


Fig. 12 Comparison of NO removal efficiency of different catalysts

desorption of NO is calculated by formula (2), and the result is shown in Fig. 12.

The removal efficiency of ACFN is only 28% at 250 °C when  $\text{NH}_3$  is introduced as a reducing gas because  $\text{NH}_3$  is a polar molecule, and compared with NO, ACFN has a higher affinity for  $\text{NH}_3$ .  $\text{NH}_3$  and NO competitive adsorption occurs on the surface of ACFN, resulting in a large amount of NO being released. Removal of NO by ammonia mainly involves the following reactions:



Under anaerobic conditions, only the reaction of formula (7) is present, and the chemical reaction rate is very low. Both FM-ACFN and CFM-ACFN occur in the low-temperature SCR reaction of manganese-based catalysts reported by Qi [13] and Pena [14] and rely on the conversion between different valence oxides of manganese to form Labie oxygen, accelerating the catalytic reduction of NO. The addition of  $\text{Fe}_2\text{O}_3$  broadens the temperature range in which the manganese-based catalyst participates in the reaction and simultaneously plays a role in oxygen storage with  $\text{CeO}_2$ , which accelerates the catalytic reduction of NO. Therefore, the efficiency of NO removal by FM-ACFN and CFM-ACFN at 250 °C is relatively increased by 12% and 14%, respectively, compared with that of ACFN.

On the catalyst surface, the adsorption of NO and the selective catalytic reduction of NO are present at the same time. NO and  $\text{NH}_3$ , as well as  $\text{NO}_2$  produced during oxygen-containing conditions, are adsorbed by ACFN, and some of the NO is oxidized to  $\text{NO}_2$  on the surface of ACFN. At the same time,  $\text{NH}_3$  will selectively catalyze the reduction of NO and  $\text{NO}_2$  in the adsorption state through chemical reactions (7)–(9). At this time, the free NO,  $\text{NO}_2$ , and  $\text{NH}_3$  will be quickly absorbed by the ACFN to fill the vacancies. In the reaction system,  $\text{NH}_3$  also directly catalyzes the reduction of NO and  $\text{NO}_2$  that are not adsorbed by ACFN. The main pathway of NO adsorption and catalytic reduction is shown in Fig. 13, where  $\text{NO}_{(\text{ad})}$  and  $\text{NO}_{2(\text{ad})}$  represent NO and  $\text{NO}_2$  in the adsorption state, respectively.

### 3.7 Removing NO by CFM-ACFN Under Different Operating Conditions

The efficiency of NO adsorption and removal by CFM-ACFN catalyst at 50–300 °C was studied under different gas distribution conditions, and the results are shown in Fig. 14.

In the pure  $\text{N}_2$  environment, the treatment of NO by CFM-ACFN catalyst mainly relies on its adsorption force and ACFN self-oxidation and reduction of NO. After the introduction of  $\text{NH}_3$ , there are competitive adsorption and low chemical reaction rates of NO and  $\text{NH}_3$  on ACFN. The catalytic efficiency has not increased significantly, and the reasons for this are analyzed in Sect. 3.5. Chemical reactions

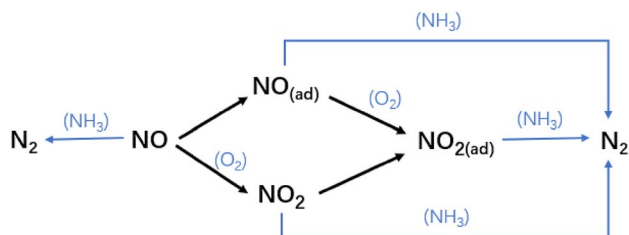


Fig. 13 Main pathways for NO adsorption and catalytic reduction

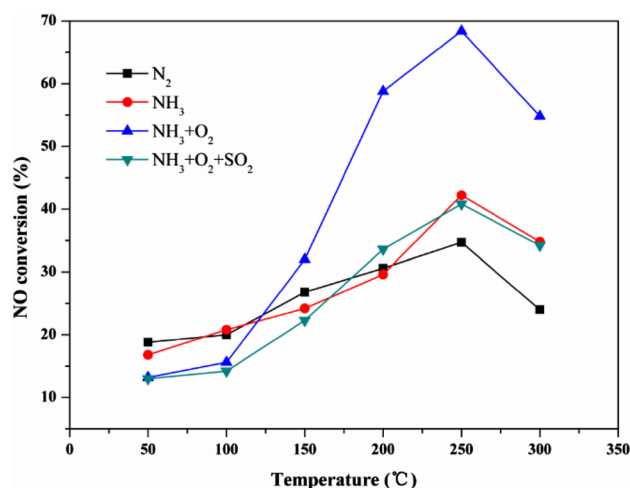
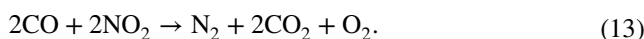
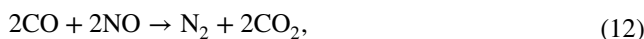


Fig. 14 Comparison of removal efficiency of  $\text{NO}_x$  under different operating conditions of CFM-ACFN

(8) and (9) occur in a system containing both  $\text{NH}_3$  and  $\text{O}_2$ , and the activation energy required for reaction (9) is only 25.2 kJ compared to the activation energy of 73.5 kJ/mol required for reaction (7) [15]; the latter reaction rate is larger than the former. Moreover, in the presence of oxygen, oxygen also adheres to the ACFN, and the percentage of oxygen in the reaction is much greater than that of NO. This result shows that in this catalytic system, CFM-ACFN, acted as a catalyst to promote the reduction of NO by  $\text{NH}_3$ . Meanwhile, ACFN also oxidatively decomposed and had a gas-phase reaction with NO to form  $\text{CO}_2$  [16]; the reaction formulas are expressed as follows:



At this time, the NO removal efficiency reached 68% at 250 °C, and it is stable. When the system contains  $\text{NH}_3$ ,  $\text{O}_2$ , and  $\text{SO}_2$ ,  $\text{SO}_2$  competes with NO and  $\text{NO}_2$  on ACFN, resulting in a rapid decrease in the adsorption capacity of ACFN for NO. Moreover,  $\text{SO}_2$  causes a part of the metal oxide to form sulfate, and the catalyst denitrification efficiency also drops remarkably.

### 3.8 Resistance of Ce to Sulfur Poisoning of Catalysts

The efficiency of adsorption and the removal of NO by FM-ACFN and CFM-ACFN catalysts under oxygen-containing sulfur at 300 °C were studied under the same gas-distribution conditions. First, the two catalysts were separately placed in the reactor, and the efficiency of treating NO in

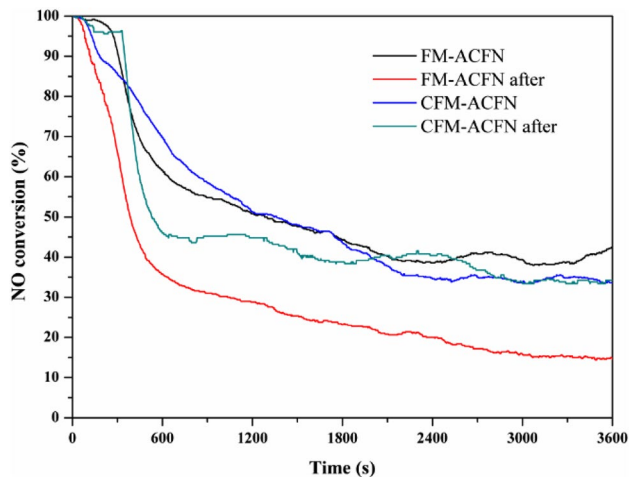


**Fig. 15** Ability of CFM-ACFN and FM-ACFN to resist sulfur poisoning

1 h was studied under the condition of oxygen-containing sulfur. Then, after the two catalysts were separately reduced by  $\text{NH}_3$ , the second treatment of NO was carried out under the same working conditions, and the results are shown in Fig. 15.

The presence of  $\text{SO}_2$  has an obvious poisoning effect on both FM-ACFN and CFM-ACFN catalyst. The NO removal efficiency of FM-ACFN catalyst decreases from 44 to 16% in the second removal, while under the same test conditions, the CFM-ACFN catalyst had the same efficiency of desorption of NO as during the previous hour and remained at approximately 42%.

Wang et al. [17] studied the reasons that  $\text{CeO}_2$  can improve the ability of the catalyst to resist sulfur poisoning in detail. The sulfur resistance mechanism of  $\text{CeO}_2$  is shown in Fig. 16.

$\text{CeO}_2$  can improve the sulfur toxicity of the catalyst mainly because  $\text{CeO}_2$  can form  $\text{Ce}_2(\text{SO}_4)_3$  with  $\text{SO}_2$  on the surface of the catalyst, increase the strength of Lewis acid, and protect the manganese-based oxide from sulfation; the catalyst is maintained in a large number of active oxidation sites while still maintaining catalytic efficiency. At the same time, the addition of  $\text{CeO}_2$  can reduce the decomposition temperature of the ammonium sulfate formed on the surface of the catalyst and prevent the accumulation of ammonium sulfate on the catalyst surface [18].

To investigate the changes of physical properties, such as specific surface area, pore volume, and surface morphology of the two catalysts FM-ACFN and CFM-ACFN before and after the reaction, the two catalysts were tested by BET before and after the reaction. Table 7 lists the various physical properties of the catalyst before and after the reaction. It was found that the BET specific surface area and pore volume of the FM-ACFN catalyst decreased rapidly

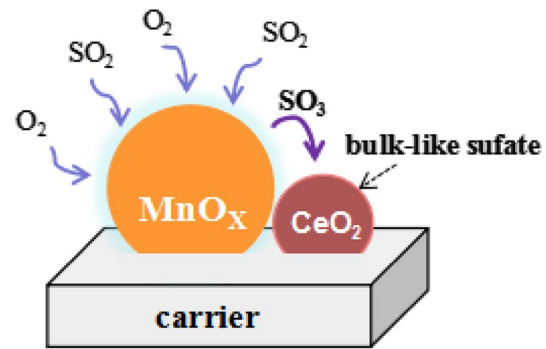


**Fig. 16** Schematic diagram of sulfur resistance mechanism of catalyst

after the reaction, and the change values were 496.22 and  $20.94 \times 10^{-2} \text{ m}^3 \text{ g}^{-1}$ , respectively. The specific values of the specific surface area and pore volume of the CFM-ACFN catalyst also decreased, but the degree of decrease is much smaller than that of the FM-ACFN catalyst. It is shown that the addition of Ce can effectively inhibit the loss of specific surface area and pore volume of the catalyst when it is reacted in a sulfur-containing atmosphere.

### 3.9 Study of Change of Gas Components Under Oxygen-Sulfur Conditions in CFM-ACFN

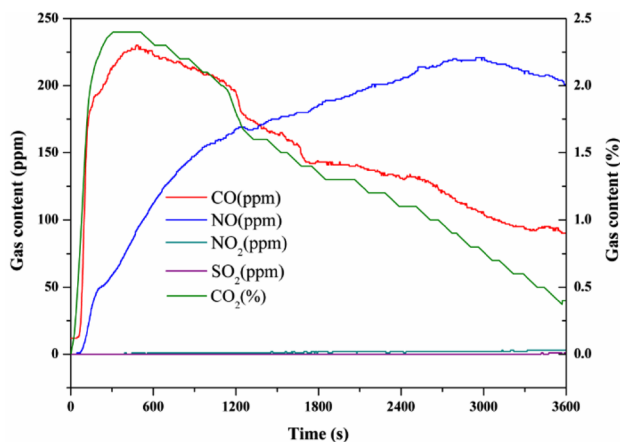
In the experiment, aMGA5 integrated flue gas analyzer was used to measure the gas components released by the CFM-ACFN removal reaction at 300 °C and containing  $\text{NH}_3$ ,  $\text{O}_2$ , and  $\text{SO}_2$ . The results are shown in Fig. 17.

It can be seen from Fig. 17 that the gas after the reaction contains a large amount of  $\text{CO}_2$  and a relatively high concentration of CO in the first 600 s, which indicates that the ACFN self-oxidation decomposition rate is high at this time. At the same time, the higher temperature causes the ACFN to release the physically adsorbed NO, and the  $\text{SO}_2$  causes the metal oxide to form sulfate to further reduce the efficiency of the catalyst, resulting in increasing NO content. Under oxygen-containing conditions, NO can be converted into  $\text{NO}_2$ , and  $\text{NO}_2$  is a polar molecule, which is easily adsorbed by ACFN to form adsorbed  $\text{NO}_2$ ; thus, the detected  $\text{NO}_2$  gas is rare.

$\text{SO}_2$  could not be detected after the reaction because  $\text{SO}_2$  is also a polar molecule, and there is a competitive adsorption relationship with  $\text{NO}_2$  and  $\text{NO}_x$  on the surface of ACFN, and the affinity  $\text{SO}_2 > \text{NO}_2 > \text{NO}$ . The presence of  $\text{SO}_2$  reduces the chemical adsorption of ACFN by NO and  $\text{O}_2$ , resulting in a decrease in the oxidative decomposition and redox NO efficiency of ACFN over time. At this time, the  $\text{CO}_2$  and CO content in the gas after the reaction shows a decreasing trend. The effect of  $\text{SO}_2$  on the ability of CFM-ACFN to deal with NO is not only to lead to sulfur poisoning

**Table 7** Physical properties of different catalysts before and after the reaction

Catalyst	BET surface area (m <sup>2</sup> /g)	Pore volume (×10 <sup>-2</sup> m <sup>3</sup> g <sup>-1</sup> )	Thickness (nm)
FM-ACFN before reaction	1110.37	66.95	2.02
FM-ACFN after reaction	814.15	46.01	2.52
CFM-ACFN before reaction	1061.02	63.75	2.14
CFM-ACFN after reaction	969.27	51.73	2.34

**Fig. 17** Variation of gas components in CFM-ACFN operating conditions containing oxygen and sulfur

of metal oxides but also to inhibit the redox NO of ACFN itself.

## 4 Conclusions

In this paper, ACF-supported metal oxide catalyst is prepared in the laboratory. The preparation processes were characterized using a thermogravimetric-differential calorimeter (TGA), and the exhaust emissions component of a diesel engine at low temperature was simulated. The catalytic efficiency of the catalyst under different gas components was analyzed. The results are as follows.

1. The addition of metal oxides CeO<sub>2</sub>, MnO<sub>2</sub>, and Fe<sub>2</sub>O<sub>3</sub> can increase the active sites on the surface of ACFN and promote the chemical adsorption of NO by ACFN. The adsorption efficiency of CFM-ACFN and FM-ACFN for NO reaches 21.5% at 250 °C.
2. The addition of metal oxides promotes the ability of ACFN in the redox reaction of NO by itself. In the presence of the reducing agent NH<sub>3</sub>, metal-oxide-loaded ACFN can increase the ability to reduce NO by approximately 14%. Under oxygen-containing conditions and in the presence of the reducing gas NH<sub>3</sub>, the metal-oxide-

loaded ACFN has a high removal efficiency for NO, which can reach 68% at 250 °C and remain stable.

3. The addition of CeO<sub>2</sub> cannot completely solve the sulfur-poisoning problem of the catalyst, but the addition of CeO<sub>2</sub> can maintain the efficiency of catalytic treatment of NO at approximately 42% in a metal-containing ACFN under oxygen-containing sulfur conditions.
4. The effects of SO<sub>2</sub> on NO treatment ability by ACFN loaded with metal oxides present two main aspects. First, for SO<sub>2</sub> competing with NO on the surface of ACFN, a decrease in the ability of the NO adsorption can be seen. Second, the presence of SO<sub>2</sub> causes sulfur poisoning of metal oxides and inhibits the redox reaction by NO of ACFN itself.

## References

1. Can F, Courtois X, Royer S et al (2012) An overview of the production and use of ammonia in NSR + SCR coupled system for NO<sub>x</sub> reduction from lean exhaust gas. *Catal Today* 197(1):144–154
2. Adapa S, Gaur V, Verma N (2006) Catalytic oxidation of NO by activated carbon fiber (ACF). *Chem Eng J* 116(1):25–37
3. Mochida I, Shirahama N, Kawano S et al (2000) NO oxidation over activated carbon fiber (ACF). Part 1. Extended kinetics over a pitch based ACF of very large surface area. *Fuel* 79(14):1713–1723
4. Yoshikawa M, Yasutake A, Mochida I (1998) Low-temperature selective catalytic reduction of NO<sub>x</sub> by metal oxides supported on active carbon fibers. *Appl Catal A Gen* 173:239–245
5. Huang J, Tong Z, Huang Y et al (2008) Selective catalytic reduction of NO with NH<sub>3</sub> at low temperatures over iron and manganese oxides supported on mesoporous silica. *Appl Catal B* 78(3–4):309–314
6. Wu Z, Jin R, Wang H et al (2009) Effect of ceria doping on SO resistance of Mn/TiO<sub>2</sub> for selective catalytic reduction of NO with NH<sub>3</sub> at low temperature. *Catal Commun* 10(6):935–939
7. Junior MAA, Matsushima JT, Rezende MC et al (2017) Production and characterization of activated carbon fiber from textile PAN fiber. *J Aerosp Technol Manag* 9(4):423–430
8. Gao ZM, Yue WU, Mei T (1996) NO Reduction by surface oxygen-containing groups on active carbons. *Chem Res Chin Univ* 17(6):961–964
9. Raymundo-Pinero E, Cazorla-Amoros D, Linares-Solano A (2003) The role of different nitrogen functional groups on the removal of SO<sub>2</sub> from flue gases by N-doped activated carbon powders and fibres. *Carbon*. 41(10):1925–1932

10. Guo J, Lua AC (2000) Preparation of activated carbons from oil-palm-stone chars by microwave induced Carbon dioxide activation. *Carbon* 38(14):1985–1993
11. Guo Y, Zhao J, Zhang H et al (2005) Use of rice husk-based porous carbon for adsorption of Rhodamine B from aqueous solutions. *Dyes Pigm* 66(2):123–128
12. Yoon KS, Ryu SK (2010) Removal of NO using surface modified activated carbon fiber (ACF) by impregnation and heat-treatment of propellant waste. *Korean J Chem Eng* 27(6):1882–1886
13. Qi G, Yang RT, Chang R (2004) MnO<sub>x</sub>-CeO mixed oxides prepared by co-precipitation for selective catalytic reduction of NO with NH<sub>3</sub> at low temperatures. *Appl Catal B* 51(2):93–106
14. Pena DA, Uphade BS, Reddy EP et al (2004) Identification of surface species on titania-supported manganese, chromium, and copper oxide low-temperature SCR catalysts. *J Phys Chem B* 108(28):9927–9936
15. Guan B, Lin H, Cheng Q et al (2010) Synergistic reduction of NO<sub>x</sub> from diesel engine exhaust by non-thermal plasma facilitated NH<sub>3</sub>-SCR. *J Eng Thermophys* 31(10):1767–1771
16. Zeng Zheng, Pei Lu, Li Caiting et al (2012) Selective catalytic reduction (SCR) of NO by urea loaded on activated carbon fibre (ACF) and CeO<sub>2</sub>/ACF at 30 & #xB0;C: The SCR mechanism. *Environ Technol Lett* 33(11):7
17. Wang Y, Li X, Zhan L et al (2016) Effect of SO<sub>2</sub> on activated carbon honeycomb supported CeO<sub>2</sub>-MnO<sub>x</sub> catalyst for NO removal at low temperature. *Ind Eng Chem Res* 54(8):150211102045005
18. Yoshimura Y, Yasuda H, Sato T et al (2001) Sulfur-tolerant Pd-Pt/Yb-USY zeolite catalysts used to reformulate diesel oils. *Appl Catal A* 207(1):303–307

**Publisher's Note** Springer Nature remains neutral with regard to jurisdictional claims in published maps and institutional affiliations.

## Affiliations

Boru Zhang<sup>1</sup> · Weijun Liu<sup>1</sup> · Furong Liang<sup>1</sup> · Shuhua Zhang<sup>2</sup>

✉ Weijun Liu  
lwj1119@139.com

<sup>2</sup> School of Chemistry and Chemical Engineering, Shanghai University of Engineering Science, Shanghai 201620, China

<sup>1</sup> School of Mechanical and Automotive Engineering, Shanghai University of Engineering Science, Shanghai 201620, China